Fluorine: Characteristics, Chemistry and Applications Controlled fluorination using atomic fluorine

Marc Dubois, Nicolas Batisse, Katia Guérin, Philippe Thomas

Fluorine: Characteristics, Chemistry and Applications

Controlled fluorination using atomic fluorine

Marc Dubois[1], Nicolas Batisse[1], Katia Guérin[1], Philippe Thomas[2]

[1]Université Clermont Auvergne, CNRS, Institut de Chimie de Clermont-Ferrand (ICCF) 24 avenue Blaise Pascal, 63178, Aubière, France
[2]Université des Antilles, Groupe de Technologie des Surfaces et Interfaces, Faculté des Sciences Exactes et naturelles, 97157, Pointe-à-Pitre, France

Introduction

Among covalent chemistry of carbonaceous nanomaterials (0D carbon blacks, 1D nanotubes, 2D graphene), fluorination is one of the most studied and important ways. Not only is fluorination a good starting point for further covalent sidewall modification of CNTs (alkylation, hydroxylation, amino-functionalization, ...) but fluorinated nanocarbons (nanoC) also exhibit a large range of possible applications themselves. Fluorination allows dispersion of nanoC in alcoholic solvents and potential applications include electric storage as cathodes in lithium batteries, in supercapacitor electrodes, sensors, and solid lubricants. Direct fluorination using pure fluorine gas F_2 remains the most useful method to obtain fluorinated carbon materials thanks to the high reactivity of molecular fluorine. However, this latter becomes a disadvantage when a F/C fluorine content lower than one is required or when the starting material exhibits high specific surface area and/or amorphous character.

In this chapter, we focus on an alternative fluorination way using fluorinating agents (FA), called controlled fluorination. The fluorinating agents such as terbium tetrafluoride TbF_4 and xenon difluoride XeF_2 are useful due to their thermal decomposition which produces atomic F and/or molecular F_2. This makes possible to progressively release a definite quantity upon the fluorination duration and thus to control both the reactivity with fluorine and the fluorine level. Whatever the dimensionality (0D carbon blacks, 1D nanotubes, 2D nanodiscs) and the number of walls for nanotubes (SWCNT, MWCNT), a higher homogeneity of the materials was obtained by this controlled process by comparison with the direct fluorination by fluorine gas. In other words, fluorinated and non-fluorinated part are homogenously dispersed. That can be explained by the low kinetic of decomposition of FA which allows a continuous addition of fluorine to carbon matrix and a more progressive fluorination. The maintaining of

a consequent fraction of residual non-fluorinated nanocarbon allows electrochemical performances to be enhanced as it could allow an increase of the electrical conductivity and as a consequence higher available current densities. The tribological properties were also improved when atomic $F^{\bullet}$ is used instead of F_2.

Fluorination with FA is also efficient to prepare carbide derived carbon (CDC) using silicon carbide as precursor, to modify the surface chemistry of many electrochemical materials such as $Li_4Ti_5O_{12}$ LTO or to change physicalchemical properties (gaz barrier, printability) of commercial polymers (polyethylene).

1. Release of atomic fluorine : thermodynamic aspects

2. Fluorination of carbon nanotubes: control of the fluorine dispersion

1.1 1D from SWCNTs to carbon nanofibres

XeF_2 thermal decomposition results in atomic fluorine F•. With DFT, F• addition to the nanotube was simulated[1]; no addition barrier was found with a F• binding energy of 54.88 kcal/mol. As a consequence, fluorine atom addition is spontaneous, and fluorine distribution on the nanotube surface is simply controlled by the electrostatic repulsion between an incoming fluorine atom and any fluorine already present on the nanotube surface. F• addition to SWCNTs is then homogenously distributed. For the case of reaction with F_2, catalytic effect of HF molecules must be considered[2]. HF molecules are only present on the nanotube surface in the presence of pre-existing fluorinated regions, and hence will only be able to catalyze further tube fluorination through F_2 addition in these regions. The fluorination mechanism with F_2 tends to aggregate fluorine atoms on the surface of SWCNTs with the formation of bands of fluorine atoms (Fig. 1a)[1,3].

Solid state NMR was performed to confirm those different distributions of F atoms along the tubes according to the reactive species (Fig. 1b). In the case of fluorination with XeF_2, two types of C-F bonds coexist with ^{19}F chemical shift of -163 and -152 ppm. -163 ppm is significantly lower than that of covalent graphite fluorides, since the nanotubes are only fluorinated on their external surface, which coupled with local curvature effects prevents formation of fully tetrahedral sp^3 C. Such an effect has been experimentally found for highly fluorinated flullerenes and derivates, regarding their ^{19}F chemical shifts[4,5]. The residual sp^2 character results in a weakening of the overlapping of the hybridized lobes of carbon and the fluorine atomic orbitals. The -163 ppm value for both samples is explained by this main effect

and represents high surface density fluorination. Only SWCNTs fluorinated with XeF_2 show the second line at -152 ppm. Because fluorine atoms are homogenously dispersed over the tube surface, C−F bonds are separated by non-fluorinated carbon atoms for compositions lower than $CF_{0.5}$. Hyperconjugation may occur, and coupled with mechanical lattice resistance to formation of fully sp^3 C results in a further weakening of the covalence[6]. This explains the ^{19}F chemical shift increase from -163 to -152 ppm.

Fluorination of SWCNTs strongly affects the intensity but not the absolute shift of the resonant Raman radial breathing modes (RBM) peaks (Fig. 1c). The treatment induces a band gap opening corresponding to a progressive increase of the transition energies. A strong decrease of the overall intensity of these bands compared to the pristine SWCNTs is observed[1]. In the case of fluorination with F_2, the Raman spectrum at low fluorine contents is very similar to that of raw nanotubes with intense modes at around 250 cm^{-1}. This is attributed to a non-homogeneous fluorination of the nanotube surfaces by this method. Indeed, if SWCNTs are not functionalized, or a large part of their surface is not functionalized, their Raman signal will be similar to the signal of the pristine SWCNTs. Nanotubes located in the outer part of the bundles may be more fluorinated than in the inner part, who may be less affected. When SWCNTs are fluorinated with XeF_2 the changes in the RBM features at 514.5 nm are progressive in accordance with a homogenous distribution of F atoms along the tubes but also within the bundles contrary to the process with F_2. At higher concentrations, there are no differences between the two methods because of a large coverage of the nanotube's surface by the fluorine atoms.

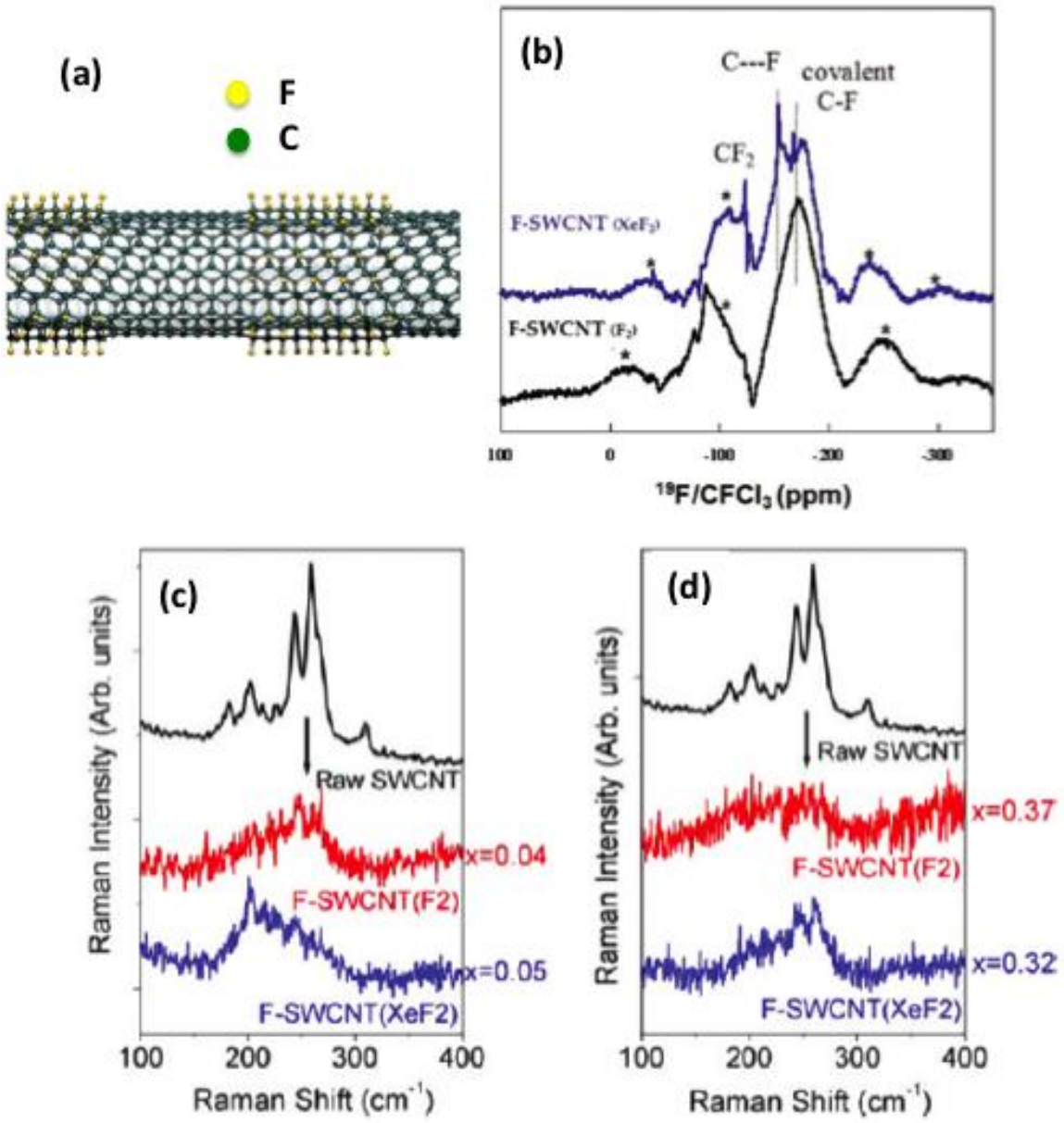

Fig. 1: a) Structures from the DFT calculations for infinitely repeating (8,8) nanotube length consisting of alternating bands of pristine nanotube segment (C_{160}) and C_2F segment ($C_{160}F_{80}$); b) ^{19}F MAS NMR spectra (at spinning speed of 20 kHz) of the SWCNTs fluorinated with F_2 and XeF_2. (*) marks spinning sidebands; c) and d) Comparison of Raman spectra at 514.5 nm between raw SWCNTs, SWCNT treated with XeF_2 (F/C = 0.05 and 0.32) and SWCNTs fluorinated with F_2 (F/C = 0.04 and 0.37). RBM massif in raw nanotubes. Arrow indicates the position of the main RBM massif in raw nanotubes.

When atomic fluorine is used, the fluorine atoms are homogeneously dispersed on the walls of the nanotubes, whatever their position in the bundle, as shown by NMR and Raman results. On the contrary, the reaction with F_2 probably starts on the defects of SWCNTs and the fluorination process then proceeds only via HF catalysis neighboring these regions, resulting

in fluorinated domains less homogeneous both in the bundles and along the tubes. Such comparison evidences the higher diffusion ability within the bundles of atomic fluorine than F_2. The study of the fluorination of carbon nanofibres (CNFs) shows that the diffusion is also efficient between the tubes. CNFs can be described as MWCNTs with a high number of walls. Moreover, they are obtained by chemical vapour deposition (CVD) and heat treated at 1800 °C in an argon atmosphere to enhance their crystallinity. Because of this crystalline order, fluorination must be performed at high temperature as for graphite. The thermal decomposition of TbF_4 was used to release atomic fluorine rather than the one of XeF_2 because it occurs at high temperature (in the 400-500°C range). The operating conditions have been optimized for TbF_4 and F_2 in order to reach similar fluorine content x in CFx, i.e. F/C atomic ratio. The fluorine contents x in CFx, after fluorination, were obtained by weight uptake and ^{19}F NMR data. The fluorination level increases regularly with the fluorination Temperature. Amongst the different samples, the highly fluorinated CNF was obtained at 500 °C for the case of TbF_4 with a corresponding fluorination level of 0.87–0.91[7]. The fluorine content were close whatever the fluorination temperature. Such agreement between the two methods is an indirect proof of both the homogeneity of the fluorinated samples and the absence of decomposition of some fluorinated parts during the fluorination. Indeed, in the case of the direct fluorination of CNFs (F_2)[8], increased reactivity of fluorine gas at high temperatures (T > 450 °C) with CNFs, leads to a competition between the fluorination and the decomposition of some fluorinated parts into volatile alkyl fluorides such as CF_4, C_2F_6,... Such duality results in an arbitrary weight loss and a high discrepancy between F/C content evaluated by NMR and the one estimated by weight uptake. This discrepancy increased with the fluorination temperature.

Scanning electron microscopy reveals differences in the morphology according to the fluorination route (Fig. 2a and b). The raw CNFs consist of a tangle of fibres with quite narrow diameter distribution, included between 80 and 350 nm. The average diameter (<Ø>) is estimated equal to 150 nm from TEM observations of various parts of the raw sample[7,8]. The fluorination results in a swelling of the fibres, moderated and uniformly located in the fibres in the case of the process with TbF_4 (atomic fluorine) (480 °C) (Fig. 2a) whereas the swelling appears larger on the raw fibre tips for CNFs fluorinate with F_2 at 480°C (Fig. 2b). Moreover, a partial exfoliation is also underlined for this later case by the presence of fibres exhibiting a drastic increase of the diameter and cracks due to the expansion. The amount of fluorine atoms into the reactor is kinetically controlled using a fluorinating agent such as TbF_4. First, the kinetic of the thermal decomposition of TbF_4 into TbF_3 could allow a

progressive release of either atomic F• or molecular F_2 fluorine. Secondly, through this decomposition, the following equilibrium is established: 2F• <-> F_2. Atomic F• is known to be more reactive than F_2 and we believe that atomic fluorine is the main fluorinating agent rather than F_2. So, atomic F• is consumed during the fluorination of carbons and the equilibrium is displaced towards the formation of atomic F•. The fluorination occurs more progressively, i.e. ‘‘sheet by sheet’’ with low structural defects amounts.

TEM bright field images of CNFs fluorinated at 420 °C with TbF_4, shown in Fig. 2, underline that the layered structure is maintained even for high temperature and high fluorine level (0.65–0.70). However, in small domains, due to the accommodation of fluorine atoms within the graphene layers (Fig. 1c and d), the interlayer distance increases from the one of raw CNFs (0.34 nm, up to the classical value of (CF)n-type graphite fluoride structure (d-spacing equal to 0.60 nm[9]). The less ordered layers, which are more spatially separated due to the accommodation of fluorine atoms, are uniformly dispersed using the fluorination at 480 °C by TbF_4 (Fig. 2d). In the case of the direct reaction with F_2, such disordered layers dispersion has not been observed at 480 °C but some exfoliation occurs. Moreover, for the lower fluorination temperature, at 420 °C for the direct (F/C = 0.39)[8] and fluorination with atomic F (Fig. 2 c and d) the distorted layers were located near the nanofibre surface[8]. This TEM study reveals at the nanoscale the first difference between the two fluorination routes.

TEM underlines also that the nanofibres length decreases at the higher temperatures, i.e. 480 and 500 °C, contrary to the low fluorination temperature (420 °C)[7,8]. A breaking of the nanofibres occurs in addition to their swelling; the average diameter increases from 150 nm for the raw CNFs to 153, 184 and 225 nm for the fluorinated samples at 420, 480 and 500 °C, respectively (these values are estimated taking into account at least 40 measurements on TEM images). TEM images of the CNFs treated with TbF_4 underline the change in the structural order during the accommodation of fluorine atoms by showing the presence of graphitic layers (Fig. 2c and d). The quantitative analysis of TEM images was performed in reciprocal space[7,8]. Any peak is observed in the two-dimensional power spectral density function (PSD) function of the fluorinated part in Fig. 2e (curve 2a in Fig. 2). A Bragg peak at about 0.34 nm in the corresponding PSD curve underlines the well-defined periodicity of the layers (Fig. 2e). The usual graphene layer periodicity found for the untreated sample graphitic structure is maintained for fluorination at 420 °C and in small amount at 480 °C. On the other hand, the PSD functions (Fig. 2 curves 2a and 3) corresponding to the entire TEM image, do not display an additional broad peak, expected with a maximum at about 1.5–2.0 nm^{-1}, which is related to the fluorinated parts although they are shown by TEM bright field images (Fig. 2c and d).

This indicates that, due to the high fluorination level obtained in the experimental conditions, i.e. (CF)n structural type, the fluorination results in a high local structural defect uniformly distributed in the whole nanofibre volume. As it does within the SWCNTs bundles, atomic fluorine may diffuse in the carbon lattice to result in homogenous dispersion of fluorine atoms. Direct fluorination with a flux of F_2 gas does not allow to reach such distribution, F atoms being concentrated near the surface for low fluorine content; then fluorination progresses from the surface towards the core[8]. It is to note that the C-F bonding is the same whatever the fluorination route, i.e. covalent, as revealed by NMR and FTIR[7,8].

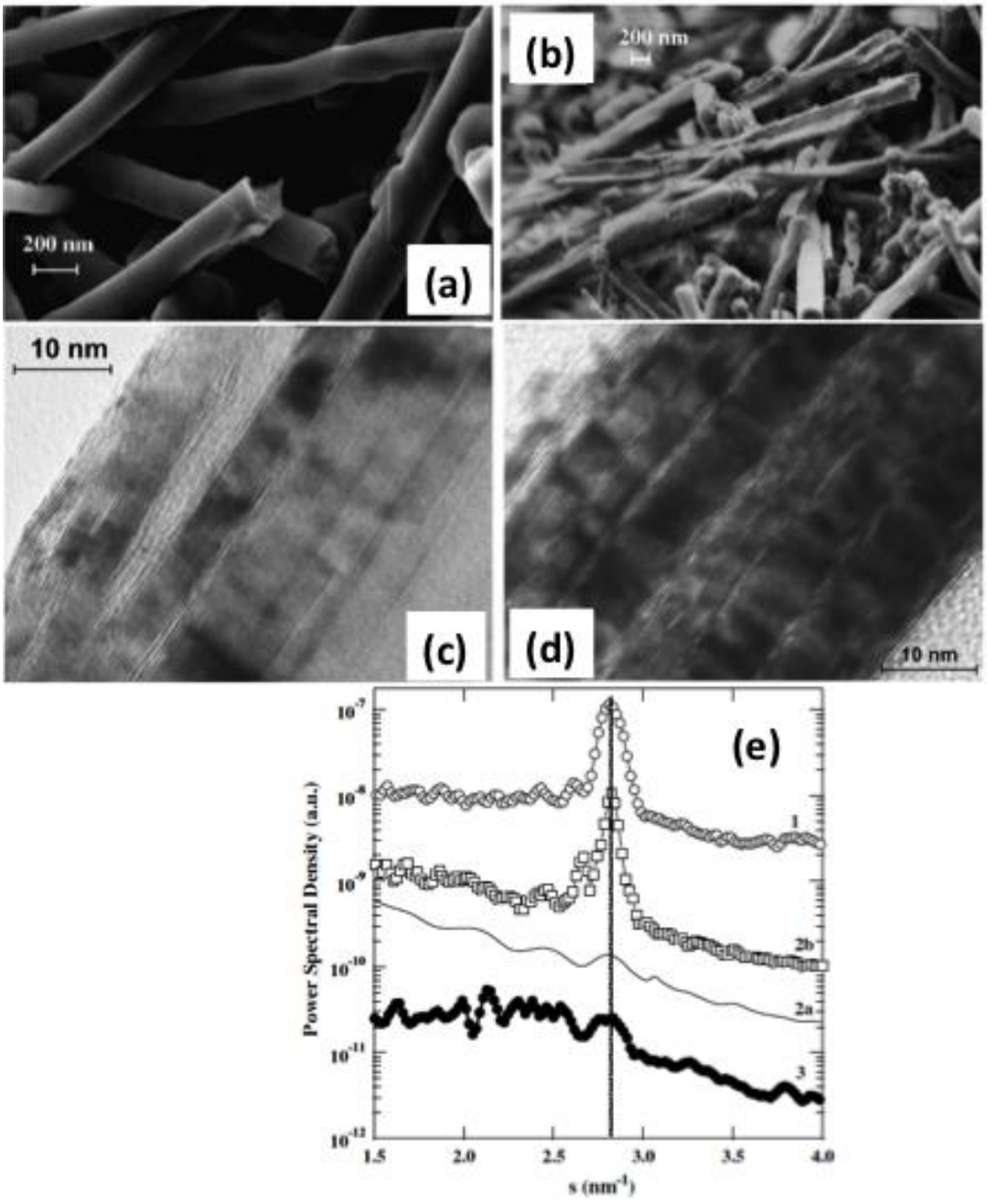

Fig. 2: SEM images of the nanofibres fluorinated with TbF_4 (a) and F_2 (b) both at 480°C; TEM images of CNFs treated with TbF_4 at 420°C (c) and 480°C (d); (e) Power spectral

density (PSD) functions calculated for the TEM images: pristine carbon nanofibres (1), fluorinated sample treated at 420 °C (2a and b) and at 480 °C (3). The curves 2a and 2b correspond, respectively, to the fluorinated part only and to entire image 2d. The curves are offset vertically for clarity. The dotted line indicates the periodicity of graphitic layers.

At this step it is important to know if the homogenous dispersion of fluorinated parts into the carbon lattice can be reached whatever the dimensionality of the carbon precursor; Fluorination of 2D carbon nanodiscs and 0D carbon black has been also investigated.

2.1 2D (nanodiscs) and 0D (carbon blacks)

The carbon nanocones and nanodiscs were produced by pyrolysis of heavy oil using the Kvaerner carbon black and hydrogen process (CBH)[10]. The CBH is an emission-free industrial process that decomposes hydrocarbons directly into carbon and H_2, based on a specially designed plasma torch, with a plasma temperature above 2000 °C. The solid output was found to consist of a significant amount of opened carbon nanocones (20 wt.%), as well as a large number of flat carbon discs (70 wt.%), and the rest being carbon black. Details about the sample may be found in ref [11]. The sample is denoted CNDs. The fluorine contents x in CFx, after fluorination, obtained by weight uptake, were 0.70, 0.95, 0.78 and 0.96 for CNDs fluorinated at 500 and 550°C with TbF_4 and 480 and 500°C with F_2, respectively. The resulting samples are called C-500, C-550, D-480 and D-500 (C and D refer to controlled and direct fluorination). Increase of the reaction temperature to 520 °C with F_2 during the direct fluorination results in partial exfoliation of the sample, which is already visible by the macroscopic volume expansion and confirmed at the nanoscale by SEM. The volume expansion due to hyperfluorination and gas evolution of volatile species such as CF_4, and C_2F_6 results in cracks and swelling on the sheet edges. This observation underlines the efficient reaction temperature range for the direct fluorination, up to 500 °C. SEM images (Fig. 3 a and b) underline the maintaining of the geometry for both fluorinations with F_2 and F, whatever the reaction temperature. Nevertheless, the disc and cone edges are more irregular in the case of 500°C with F_2. Moreover, a nanocarbon swelling occurred due to the accommodation of the fluorine atoms. This swelling differs after the direct and controlled processes as revealed by atomic force microscopy. AFM was performed in tapping mode. Topography and error images show a clear difference in the surface morphology (Fig. 3c and d). The accommodation of the fluorine atoms occurs by a swelling, which is more pronounced on the edges for the sample treated with F_2 (Fig. 3c); the maximum extent of swelling is

observed in the overall perimeter. The edge seems then to be the preferential area for the direct fluorination. On the contrary, the swelling is homogenous for CNDs treated with TbF_4 at 550°C and the accommodation of fluorine atoms results in small cracks homogenously dispersed on the disc surface. The fluorination progressively changes the structure as a function of the fluorination temperature (T_F). The XRD patterns of the fluorinated CNDs are compared in Fig. 3e. The pristine CND pattern is similar to graphite. The main peaks correspond to the graphite structure (002), (100), (101) and (004) diffraction lines for 2h values of 26.4° (interlayer distance d = 0.337 nm), 42.9° (0.211 nm), 44.8° (0.202 nm) and 54.4° (0.169 nm). CNDs exhibit a high structural organization thanks to the post treatment at 2700 °C (coherence length along the c axis, Lc = 39 and 2 nm for post-treated and raw CND, respectively). For CNDs treated with TbF_4 a new phase appears with corresponding peaks at 2h values centred at 14.8° and 40.9° attributed to the (001) and (100) peaks of a fluorographite matrix in an hexagonal system. The corresponding interlayer spacing of 0.60 nm is characteristic of (CF)n-type structure. On the contrary, an intermediate phase is deduced for D-480 and D-500. Because of the coexistence of $(C_2F)n$ and (CF)n phases, the value d equal to 0.68 nm is measured instead of 0.81–0.82 nm and 0.6 nm for $(C_2F)n$ and (CF)n structural types, respectively. Moreover, because of this coexistence of phases, the full width at half maximum is larger for D-480 and D-500 ($\Delta\theta$ = 3.7°) than for C-500 and C-550 ($\Delta\theta$ = 2.7°). The reactive species, atomic or molecular fluorine, acts also on the structural properties, C-F bonding being similar (covalent). Atomic fluorine at high temperature allows the (CF)n type to be reached whatever the F/C ratio.

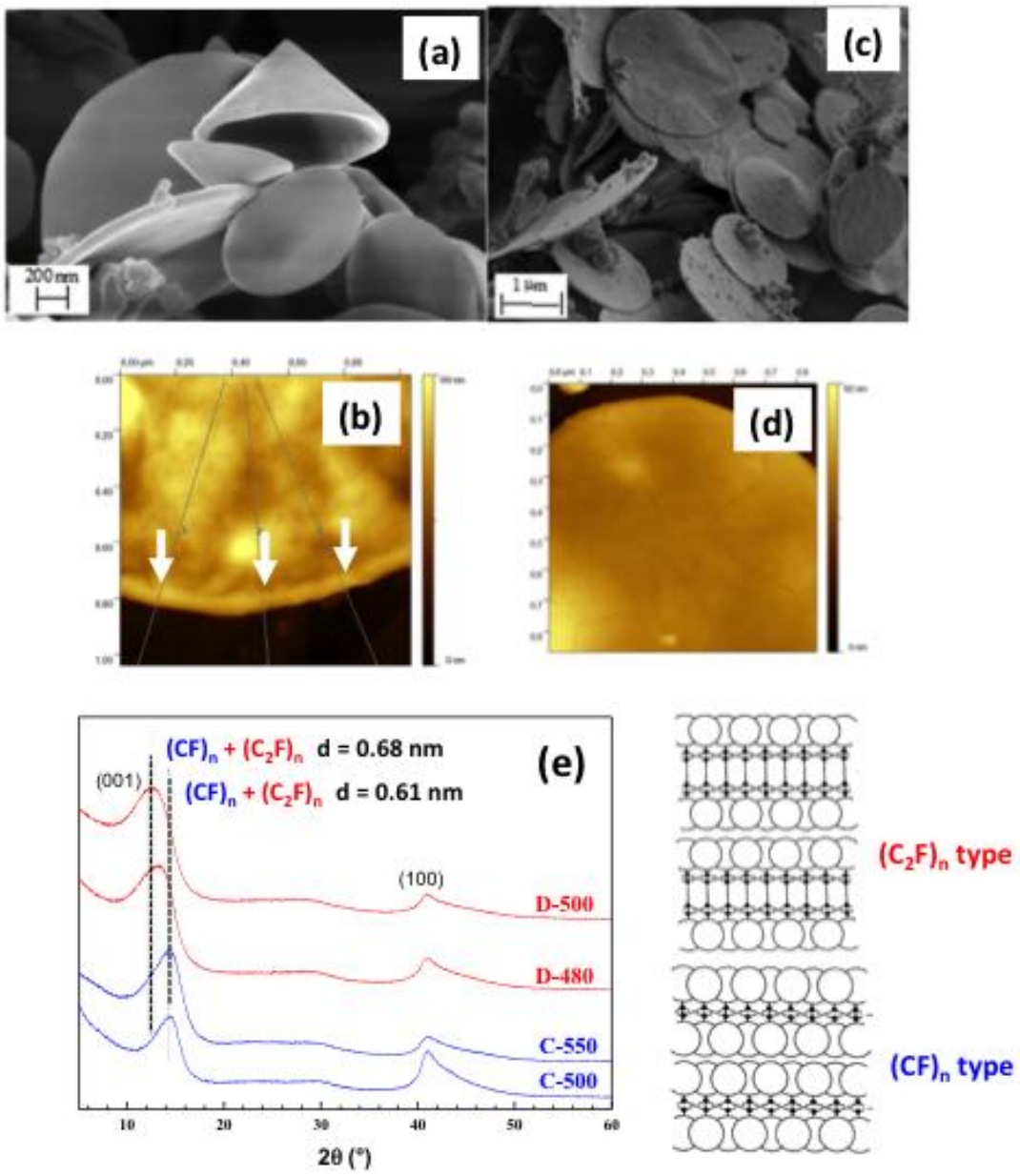

Fig. 3: SEM (a) images of the CNDs plus the highest fluorine content, i.e. C-550 (F/C = 0.95) and D-480 (F/C = 0.96); AFM images of D-500 (a), and C-500; XRD diagrams of C-500, C-550, D-480 and D-500.

Nano-sized graphitic carbon black materials (GCBs) have been developed by Superior Graphite, Chicago, Illinois and are produced by hydrocarbons pyrolysis. This commercial product is synthesized from carbon blacks by a high temperature graphitization treatment between 1500 and 3000 °C. This treatment results in the almost total elimination of the impurities (volatile species, sulfur, ash) present in the carbon black precursor and the graphitization of the carbon nanoparticles. Taking into account the particles size with an averaged value of 40 nm, the coherence length along the c-axis (Lc) is limited to 7 nm

although the graphitization treatment. The commercial products differ from other types of carbon blacks[12]. Two types of fluorinated GCBs were studied for comparison. The first one was obtained by direct fluorination under pure fluorine gas, for temperatures ranging between 380 and 440 °C (The duration of each experiment was of 3 h). The same conclusion about the structural phase than for CNDs can be extract from XRD and electron diffraction. The interlayer spacing indicate that the structure is (CF)n only, with atomic fluorine, or a mixture of (CF)n or (C_2F)n with F_2. TEM reveals the morphology and the structure of nanoparticles such as fluorinated GCBs and also to investigate the mechanisms of fluorination with F_2 and TbF_4. Numerous TEM images were recorded and the ones presented here are representative of the whole studied samples. TEM images recorded on initial GCBs and on the different fluorinated derivatives obtained with direct (F_2) fluorination are presented in Fig. 4. Images collected on initial GCB (Fig. 4a) clearly point out their graphitic structure with measured inter reticular distances of 0.34 nm corresponding to graphene interlayer distances in graphite (see electron diffraction pattern on Fig. 4b). GCBs appear as faceted nanoparticles resulting from their structure constituted of well ordered nano-domains joined by faulted regions of very small spatial extension needed to accommodate the quasi spherical shape of the nanoparticles. The faulted regions present also a high curvature of the carbon layers subjected to be more reactive with F_2 than the well organized and flat domains. As for fullerenes and derivatives (nanotubes), the curvature results in a few percentage of sp^3 hybridization in addition to sp^2 one. That decreases the stability of the carbon lattice and the reactivity toward fluorine increases[13]. As an example, C_{60} fullerenes and single-walled nanotubes may be fluorinated event at room temperature. Once opened during the fluorination process, they may play a role of access zones to fluorine atoms. Once fluorinated using the F_2 method, the first images recorded at low magnification (Fig. 4c, e, g) present swelled materials due to the inclusion of fluorine atoms. Moreover, the first sheets on the image of Fig. 4c exhibits a structural evolution caused by the fluorination[14]. The sheets are corrugated and have an interlayer distance of about 0.48 nm, which is characteristic of fluorocarbon stacking. When the fluorination level increases, fluorinated areas progress toward the core of the material. The highly fluorinated angular portions are opened when the fluorination level increases, creating by this way an opening for the insertion of fluorine atoms (Fig. 4g). The accommodation of fluorine atoms on the periphery of the particles leads to the destructuration of the fluorocarbon sheets (Fig. 4g). In the case of the controlled fluorination method, the diffusion of the atomic fluorine differs. Indeed, for similar F/C (≈0.3) the extension of the fluorinated region (corrugated layers with enhanced interlayer distances) is greater for compounds

obtained with controlled fluorination (Fig. 4d and f) than with direct fluorination (Fig. 4c and e)[14]. For higher fluorination levels, fluorinated particles obtained with controlled method do not exhibit significant structural differences with those obtained with direct method. The fluorinated parts are homogeneously distributed on the whole volume of the particles (Fig. 5h). Contrarily to the direct fluorination using fluorine gas, the controlled process is monitored by the kinetic of decomposition of TbF_4 fluorinating agent, which allows a continuous addition of fluorine to carbon matrix and a more progressive fluorination without damaging the carbonaceous lattice. The diffusion of fluorine radicals more deeply in the nanoparticles reduces the accumulation of fluorine in the outer shell layers preserving them from damaging up to high fluorination rate (F/C ≈ 0.83).

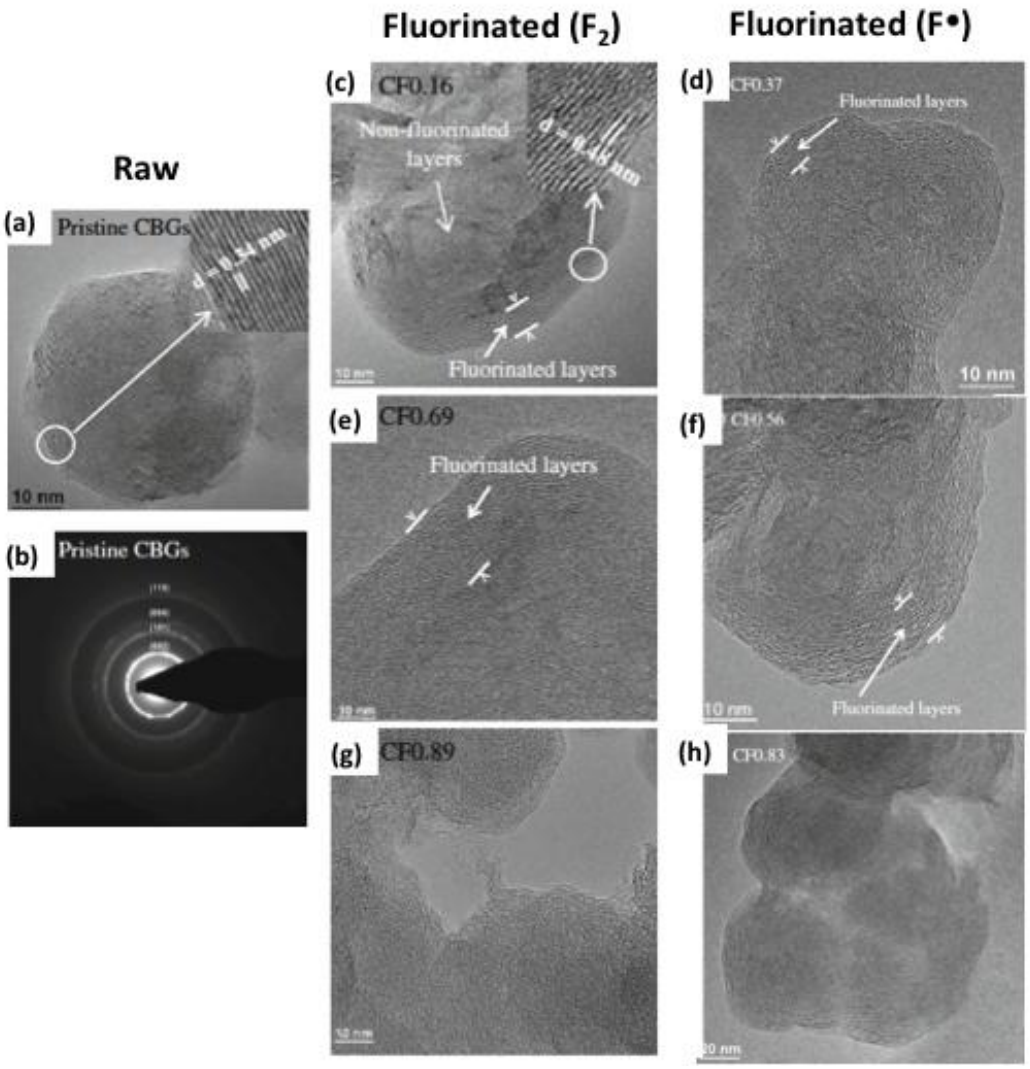

Fig. 4 : TEM images and electron diffraction pattern of GCBs, raw (a, b), fluorinated by F_2 (c, e, g) and TbF_4 (d, f, h)[14].

The fluorination route acts on the thermal stability. For a similar fluorination level, thermal stability of GCBs fluorinated with TbF_4 is greater than the sample treated with F_2. Indeed, with a high F/C (around 0.8), GCBs fluorinated by F_2 are stable up to 500 °C; on the contrary, when they are functionalized using atomic fluroine, the material is stable up to 565 °C. These differences in terms of thermal stability can be explained using TEM analyses discussed previously. Indeed, a high degree of fluorination obtained using a direct fluorination leads, as shown in the images in Fig. 4g, to the formation of fragile particles, partially divided, or delamination of the external perfluorinated layers. In the case of a fluorination controlled with TbF_4, the mechanism involving more easy diffusive F• species in the carbon structure leads to more homogeneous fluorinated materials and results in the formation of stable fluorinated particles, which are not or slightly damaged (Fig. 4h). Due to their greater density of nanometric scale defaults in their structure, the GCB fluorinated by F_2 present, when they are heated at high temperature, a higher decomposition kinetic than GCB fluorinated by the controlled process, probably due to the easier diffusion of gaseous fluorinated species (CF_4 and C_2F_6) and oxygen, through the highly faulted regions.

The fluorination route either with atomic or molecular fluorine results in different fluorine atom distributions within the carbon lattice, different structure and thermal stability. The applicative properties may be tailored or enhanced thanks to those facts.

3. Enhancement of the applicative properties

3.1. Power density in primary lithium battery with fluorinated nanofibers as cathode

3.3 Tribological properties of fluorinated carbon blacks

The tribological properties of the compounds were evaluated using a ball-on-plane tribometer consisting of an AISI 52100 steel ball describing an alternative motion on a static AISI 52100 steel plane on which the tested material was deposited. A normal load F_n of 10 N was applied, leading to a contact diameter of 140 μm (Hertz' s theory) and a mean contact pressure of 0.65 GPa. The sliding speed was 6 $mm.s^{-1}$. The measurement of the lateral force F_t allowed us to calculate the friction coefficient, expressed as $\mu = F_t/F_n$.

The balls were used as delivered whereas the surface of the planes were abraded in order to generate multidirectional scratches to improve the adherence of powdery materials. After balls and planes cleaning in ultrasonic baths in acetone and ethanol, few milligrams of GCBs were deposited on the plane surface. Then a drop of pentane (boiling point 36°C) was added

after ball on plane contact in order to improve the particle feeding of the sliding contact and accelerate the establishment of the tribofilm.

The intrinsic tribologic properties of the tested materials in air (relative humidity: 50 ± 5%) were obtained after total pentane evaporation (occuring after few cycles). One friction cycle corresponds to one reciprocal travel of the ball on the plane.

The friction properties of three fluorinated GCBs obtained from direct fluorination and three compounds resulting from controlled fluorination were evaluated. The corresponding fluorine contents are reported in Table 1.

	Direct fluorination			Controlled fluorination		
T_F (°C)	360	380	400	320	410	480
Duration	3h	3h	12h	12h	12h	12h
F/C	0.16*	0.69*	0.89^{+}	0.37^{+}	0.56*	0.83^{+}

Table 1: Evolution of the fluorine content as a function of the fluorination temperature T_F for direct and controlled fluorination methods. The fluorine content is expressed as atomic F/C ratio determined from weight uptake (*) and quantitative ^{19}F NMR ($^{+}$).

Fig. 5 presents the evolution of the intrinsic friction coefficient in air of fluorinated GCBs obtained from direct and controlled fluorination as a function of F/C content. The intrinsic friction coefficient of pristine GCBs is similar to that of graphitized carbonaceous structures ($\mu = 0.12 \pm 0.03$). Fig. 5 shows that fluorination strongly improves the tribological properties of GCBs whatever the fluorination method. A linear decrease of the friction coefficient as a function of F/C is observed for low fluorine contents down to an asymptotic value for higher F/C ratios. In the case of direct fluorination, $\mu = 0.085 \pm 0.005$ for F/C > 0.6. The friction coefficients recorded for fluorinated GCBs obtained with atomic fluorine are lower than the ones obtained from molecular fluorine, whatever the fluorination level. Moreover, a very low asymptotic value of μ is obtained with controlled fluorination ($\mu = 0.065 \pm 0.002$). The lubricating performances of fluorinated GCBs consequently appear to be strongly enhanced if following the controlled fluorination method compared to direct one.

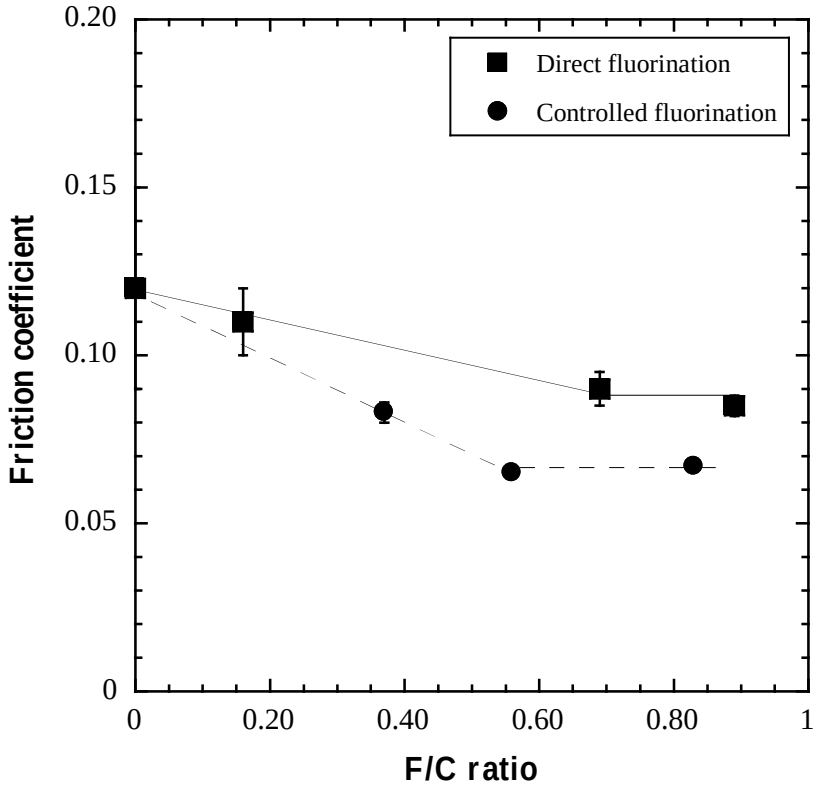

Fig. 5: Evolution of intrinsic friction coefficient in air (recorded at 3 cycles after pentane evaporation) as a function of F/C ratio for fluorinated GCBs obtained from direct and controlled fluorination.

As already described in the case of other carbon compounds[15], the friction reduction mechanisms are attributed to surface effects, i.e. to interparticles interactions. Indeed, fluorinated particles present lower surface energy than pristine ones leading to lower friction coefficient values. During the fluorination process, the thickening of the fluorinated region (see Fig. 4) lowers the surface energy of GCBs resulting in a decrease of the friction coefficient. When the fluorinated region is thick enough to stabilize the surface energy of fluorinated GCBs, the interparticles interactions do not evolve any more, leading to a stabilization of the friction coefficient. A fluorinated shell thickness, determined from TEM images, close to 10 nm is needed to stabilize the friction coefficient[14].

The improvement of the tribological behavior of fluorinated GCBs observed with controlled fluorination can be explained considering TEM characterization of the compounds. For similar F/C contents, the extension of the fluorinated layers is greater for compounds obtained with controlled fluorination (see Fig. 4) compared to direct fluorination. For low fluorine contents, the interparticles interactions are consequently lowered with controlled fluorination, resulting in lower friction coefficients. In the case of high fluorination levels, the friction

coefficient values are higher with direct fluorination than with controlled fluorination. This is probably due to the fluorination process: direct fluorination induces damaging of the particles contrarily to controlled fluorination for which the initial spherical shape of the particles is maintained.

In order to evaluate the influence of the friction process on the tribological properties of fluorinated GCBs obtained from controlled fluorination, long-term friction experiments were performed. Fig. 6 shows the evolution of the friction coefficient, as a function of fluorination content, recorded after 1000 cycles of friction, in comparison with the intrinsic ones.

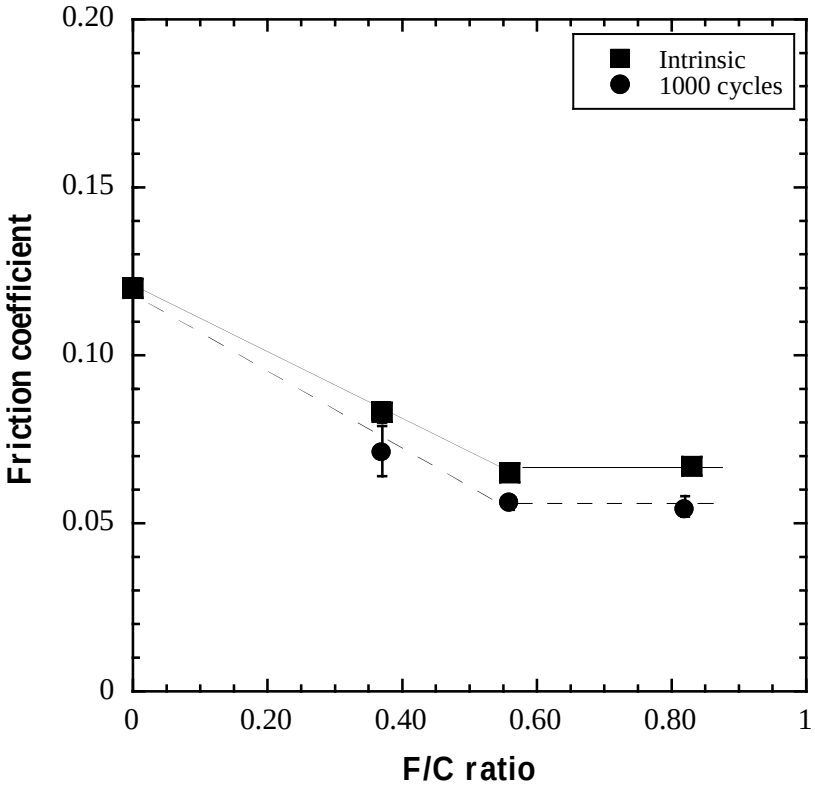

Fig. 6: Evolution of the friction coefficient recorded at 3 cycles (intrinsic friction coefficient) and at 1000 cycles after pentane evaporation as a function of F/C ratio for fluorinated GCBs obtained from controlled fluorination.

Fig. 6 shows a decrease of the friction coefficient during the friction process down to a value close to 0.06 for high fluorine contents. During the friction process, particles are broken and partially defluorinated and the structure of the tribofilm, composed of fluorinated carbon phases dispersed in a graphitic matrix, is established after 200 cycles[15]. If surface effects are involved in the friction reduction mechanisms at the beginning of the friction tests, the bulk

properties of the tribofilms seem to ensure the good lubricating performances of fluorinated GCBs, obtained from controlled fluorination, for long-term experiments.

Fluorinated GCBs obtained from controlled fluorination appear as interesting candidates to be used as new friction reduction nano-additives for lubricants. In addition to good intrinsic properties, the size and morphology of the particles are well adapted for a good feeding of the sliding interface and the possibility to obtain stable dispersions in gel or liquid lubricants.

4. A general route efficient for…

4.1 for polymers

XeF_2 is easily decomposed on the polymer surface even at room temperature. Nevertheless, the temperature was increased in order to enhance its vapour pressure and the reactions take place. XeF_2 and polymer films were deposited in the reactor in a glove box under argon atmosphere. Then, a closed reactor under Ar was stored at a constant temperature of 60 °C for 48 h. The direct fluorination using molecular fluorine F_2 was carried out at room temperature. Open reactor with continuous F_2 flow at ambient pressure was used. In a typical experiment, LDPE samples were placed inside reaction Nickel vessel in an alumina cylindrical support. The sample is denoted F_LDPE_DF (DF for direct fluorination, when a number is indicated it corresponds to the treatment duration). The PE treated with XeF2 is called F_LDPE_XeF_2.
The two fluorination routes exhibited different reactivity, the processes being clearly different due to the use of different fluorine reactant, molecular (F_2) and atomic (F•). As for carbonaceous nanomaterials, the reactivity directly depended on the diffusion kinetics of the fluorine species on the surface or in the treated polymer bulk. For the sample treated at direct fluorination conditions (F_2), an upper fluorinated layer consisted mainly of specific fluorinated groups like -CF_2-. Some polar groups have been also detected. Several sources could explain this fact during the treatment process or after the reaction during exposure to air. Some C-H and C-C bonds could be broken during the fluorination processes, forming dangling bonds, which could react either with the oxygen and moisture from air or O_2 admixtures in F_2 or O_2 and H_2O absorbed on the surface and in the bulk. For the process performed with XeF_2, where atomic F• is the main fluorinating species, specific groups (-CHF-) were detected not only on the polymer surface but also in the bulk. The final CHF/CF_2 ratio depended on the fluorination route. F• resulted in a prevailing formation of -CHF- groups in bulk whereas F_2 formed mainly -CF_2- groups. The relative content of those groups were extracted from both infrared spectroscopy and solid state NMR[16]. Fluorinated polymers

surface composition and the CHF/CF_2 ratio have been also derived from the C1s core peaks represented in Fig. 5a. The sample surface was oxygenated and its content depended on the fluorination route nature. From the quantitative analyses, 14% of oxygen were detected for the direct fluorination with F_2 routes and XeF_2 routes. We have to note that the pristine polymer contained 3% of oxygen atom due to the oxidation processes during fabrication and storage. The binding energy was clearly shifted towards the high values after fluorination process (+1.0 eV). Two components have been identified, one located at 532.5 eV was assigned to C=O environments and another at 533.8 eV was attributed to oxygen atoms C-O-C environment. Pristine and fluorinated LDPE C1s core peaks exhibited five to six components depending on the fluorine route. In agreement with literature[17] (see tables in Fig. 5). For the case of dynamic fluorination process, an important increase of the carbon component at 290.5 eV assigned to the $CF-CF_2$ environment was recognized, with the fluorination time and with a smaller input of the component at 292.8 eV attributed to CF_2-CF_2 environment. For the samples fluorinated with XeF_2, most of the groups detected were attributed mainly to –CHF-. It is important to keep in mind that this analysis was performed on the utmost surface layer thinner than 5 nm.

Those two kinds of processes have been revealed two different mechanisms which could be devoted to different macroscopic properties, both on surface or in the bulk such as tribological properties or gas permeability.

Polar (γ_{Polar}) and dispersive ($\gamma_{Dispersive}$) components as well as a total surface energy allow the printability to be quantified. Water and formamide were used to measure total surface energy and polar and dispersion components in the frame of conventional Owens–Wendt methods. Fig. 5b, c and d depict the contact angles of the two liquids measured just after experiments on the fluorinated surface treated in dynamic conditions (flux of F_2) and with XeF_2. It was recognized that the total surface energy and its polar and dispersive components depended mainly on the type of fluorination routes[18]. These three parameters have been markedly increased in the case of the samples fluorinated in dynamic conditions (F_LDPE_DF). Usually, surface tended to become more hydrophilic after fluorination treatment. The dispersive component increased from 17.3 (Pristine LDPE) to 41.7 mN/m (F_LDPE_DF020, 20 means 20 min). It is well known that the surface energy of fluorinated polymers is increased after direct fluorination processes using molecular fluorine as a reactant, also adhesion and printability properties should be enhanced[19]. First, the polar component have been increased due to the formation of specific polar groups such as -(C=O)OH, -CHF- and -FC=O, on the polymer surface in dynamic conditions. Oxygen played also a key role on this

increase; several sources could be described during the process or after the reaction during the exposure to air. Some C-H and C-C bonds could be broken during the fluorination processes, forming dangling bonds, which reacted with oxygen and moisture from air. Oxygen containing bonds could be formed in the course of fluorination due to a technologic admixture of oxygen in used fluorine or O_2 and H_2O absorbed on a polymer surface and reactor walls. Also the surface roughness was increased under fluorination which also resulted in a surface energy increase. For the process using the specific fluorinating agent XeF_2, polar component has been increased and exhibited that the surface has been covered with different polar groups defined by the previous analyses. Finally, it is also important to note that the fluorination increased the roughness of the polymer surface. On the contrary, the gaseous flux resulted in an excess of F_2 gas at the surface resulted in higher density of dangling bonds, which react with oxygen, and higher roughness due to the hyperfluorination and possible polymer chains scission[20]. Influence of storage duration on the surface parameters was also studied for F_LDPE_DF020 and F_LDPE_XeF_2 (Fig. 5). The surface of the sample treated in dynamic conditions and with XeF_2 exhibited the tendency to become more hydrophilic for a defined period (≈10 days). This behaviour indicated that on optimum time could be followed in order to identify the maximum printability.

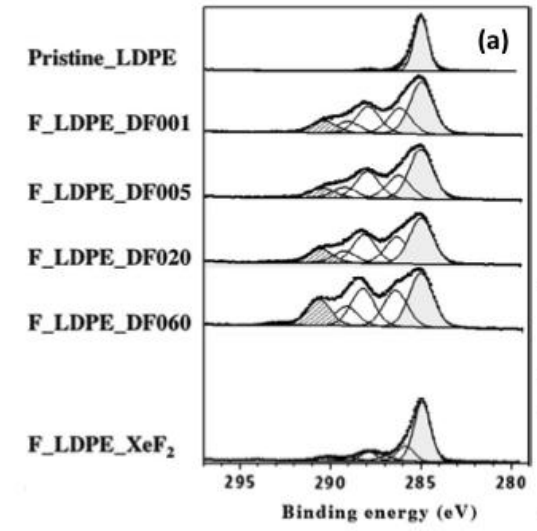

Contributions	Assignments	Energy (eV)	ΔeV
C1s A	CH_n	285.0	**0**
C1s B	CH_2–CF_2	286.3	**1.3**
C1s C	CHF–CH_2	288.1	**3.1**
C1s D	CHF–CF_2	289.3	**4.3**
C1s E	CF_x–CF–CF_2	290.6	**5.6**
C1s F	CF_2–CF_2	292.7	**7.7**

Contributions	Assignments	Energy (eV)	ΔeV
C1s A	CH_n	284.9	**0**
C1s B	CH_2–CHF	285.8	**0.8**
C1s C	CHF–CH_2	287.9	**3.0**
C1s D	CF_x–CF–CF_2	290.05	**5.38**

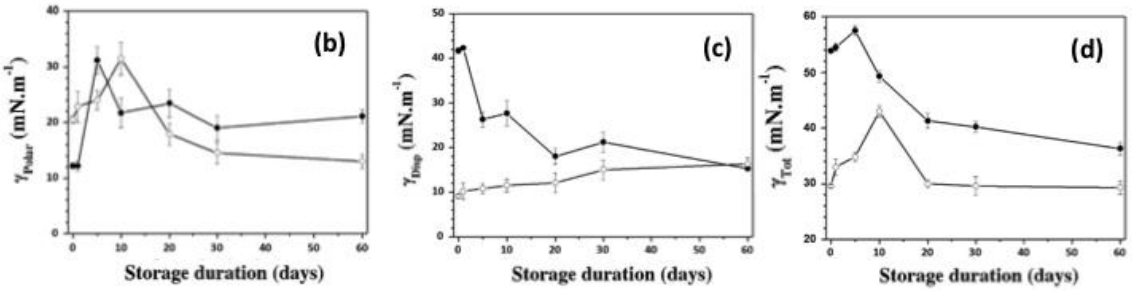

Fig. 5: (a) C1s core XPS spectra of pristine and fluorinated LDPE (F_2 for 1, 5, 20 and 60 min and XeF_2); Evolution of the polar (b), dispersive (c) components and total surface energy (d) vs storage duration of fluorinated LDPE treated in F_2 dynamic conditions (●) and with XeF_2 (○).

4.2 Synthesis of fluorinated monolayer graphene

Absence of the gap in the band-structure of graphene results in significant limitation in its use in electronics. One direction to overcome this drawback is functionalization of graphene with suitable elements, such a s hydrogen and fluorine. A planar crystal structure is then obtained, with bonds between the sp^2 carbon atoms, into a three-dimensional structure with sp^3 bonding between them. Theoretical predictions show that hydrogen and fluorine are good candidates to play such a role; band gaps of 3.8 eV and 4.2 eV is expected for 100% functionalization, respectively[21]. Nowadays, three types of synthesis methods are mainly employed to obtain fluorinated graphene; all require mild conditions as follows: i) Fluorographene or fluorinated graphene have been synthesized by exposing graphene in XeF_2 or diluted F_2 atmosphere[22]. Even if this method can prepare high-quality fluorinated graphene, the higher cost and the needed control of the reaction do not permit the large-scale production of this material. ii) Very recently, fluorinated graphene has been prepared by fluorination of graphene oxide with fluorhydric acid HF[23] 20 or F_2[24]. However, FG sheets obtained by this approach show an irregular atomic arrangement compared to the theoretical crystal structure of fluorographene. The total substitution of oxygen atoms by fluorine ones is difficult and the resulting samples appear as graphene oxifluoride rather than fluorographene. It is clear that all aforementioned methods have their respective inadequacies; iii) Exfoliation of (highly) fluorinated graphite is also efficient. Liquid-phase exfoliation methods have also been carried out in organic solvents such as chloroform[25] or N-methyl-2-pyrrolidone[26]. This method possesses two main drawbacks: the solvent used is often toxic, and the process needs a considerable period of sonication to be efficient. In addition, some studies concerning the exfoliation using ionic liquids as an intercalated species under ambient conditions was utilized to obtain fluorinated graphene[27], but the problem lies in the difficulty to eliminate efficiently the traces of residual solvent. Mechanical exfoliation from the fluorinated graphite may be performed onto conventional Si/SiO_2 substrates. For this way, the distribution of fluorine atoms in the carbon lattice is of primary importance. Homogenous dispersion favors the mechanical exfoliation. Fully fluorinated highly oriented pyrolytic graphites (CF)n were prepared by fluorination with

F_2 at 530 and 600°C as a starting materials for exfoliation. On the other hand, flakes of natural graphite was treated with XeF_2 (120 °C for 48 h). The resulting F/C ratios were 0.86, 1 and 0.28 (and 0.24), respectively. After mechanical exfoliation, AFM evidences multilayers with height of 10 nm for CF_1 and 0.86, 6.1 nm for $CF_{0.28}$. On the contrary, monolayer was obtained when XeF_2 was used as fluorinating agent. To obtain more information on the structure of the exfoliated samples, Raman spectra were measured (Fig. 6a). In addition to the analysis of D/G ratio in relation the presence of defects and residual fluorine atoms on the surface, both position and shape of the 2D band were analyzed to evidence the presence of graphene layers in the exfoliated sample and their stacking. Both the presence of fluorine atoms and the increase of the amount of defects formed during the mechanical exfoliation contribute to the high intensity of the D-band. D' band, characteristic of few layer graphene sheets, appeared as a shoulder of the G band[28]. Concerning the 2D band, it may be a direct indicator for a graphene-like sheets with few layers[29]. Fit of 2D peak by a single Lorentzian function (fwhm 30-45 cm^{-1}) underlines monolayer only for the sample prepared with XeF_2[30]. The homogenous dispersion of the F atoms obtained with atomic fluorine plays a key role.

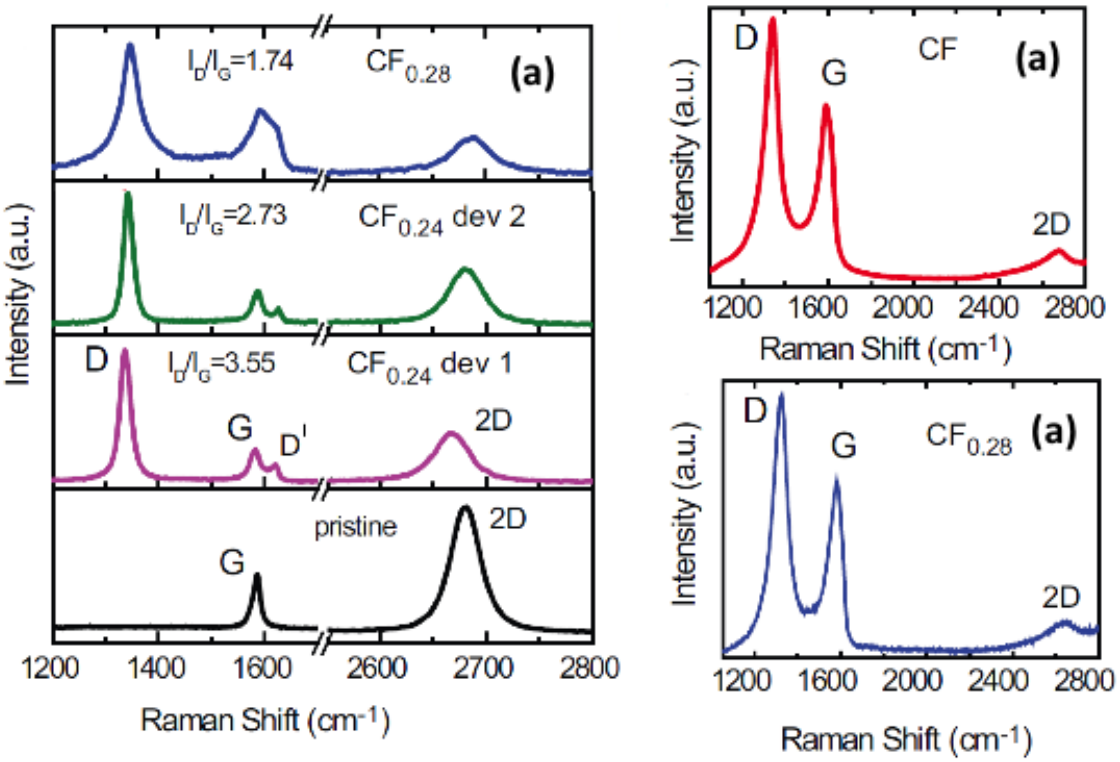

Fig. 6: Raman spectra of raw and exfoliated graphite fluoride prepared with XeF_2, (a) and exfoliated samples synthesized with F_2 (b)

4.3 Synthesis of carbide derived carbon (CDC)

Unusual thin films with bimodal dispersion of layers, i.e. both SiC and carbide derived carbon CDC-SiC, can be prepared using XeF_2 decomposition. Atomic fluorine reacts preferentially with silicon atoms and is evolved to the gas phase. FTIR spectra of samples fluorinated by XeF_2 (Fig. 7f) indicate that only carbon vibrations appear whatever the SiC/XeF_2 ratio. The two bands at 1450 and 1620 cm^{-1} are assigned to sp^2 C-C and C=C, respectively[31]. No carbon-fluorine bonds are formed contrary to fluorination with fluorine gas although the synthesis temperatures are approximately the same (120-130°C). Moreover, partial etching is possible when SiC/XeF_2 ratio is controlled; a SiC/CDC composite can be then prepared. For higher molar ratio, silicon is totally etched and higher carbon level is obtained. Such a way allows the fluorination to be controlled contrary to the direct process using molecular fluorine. Moreover, the release of SiF_4 allows a progressive cleaning of the thin films surface and this species is easily removed from the surface. The formed carbons rearrange themselves to form a real nanostructured carbon film, which is composed of graphite nanocrystallites (see SEM image in figure 7b and c). On the contrary, after fluorination with F_2, an absorption band appears at 1180 cm^{-1} in addition to the ones at 1450 and 1620 cm^{-1}. The new band is attributed to covalent carbon fluorine bonds such as in covalent graphite fluorides[32]. Whatever the fluorination method the fluorination mechanism is similar with XeF_2 and F_2 as evidenced by SEM images (Fig. 7); silicon atoms are extracted from the amorphous silicon carbide matrix which has a columnar-like structure. This results in a formation of a new thin film where carbonaceous columns represent a matrix surrounded with porous columns (Fig. 7). The porous columns are about 20 nm in diameter and allows the diffusion of both fluorine and silicon fluoride formed during the reaction. The high reactivity and excess of molecular fluorine used for direct fluorination lead to a reorganization of the porous structure which destroys the carbonaceous matrix and provokes some wrenches and folds in the thin films (Fig. 7d and e). By treatment with XeF_2, the reorganisation of the porous structure is avoided and CDC thin film surface is homogeneous. So, fluorination with atomic can be used for the synthesis of carbon thin films on carbide surfaces at lower temperatures than for the case of chlorination (the conventional method), i.e. 30-130°C. For thermodynamic simulations made for the SiC/Cl_2 system[33], the thermodynamic probability of the carbon formation increases with the reaction temperature. If one mole of silicon carbide reacts with more than two moles of chlorine, a temperature as high as 900°C is required.

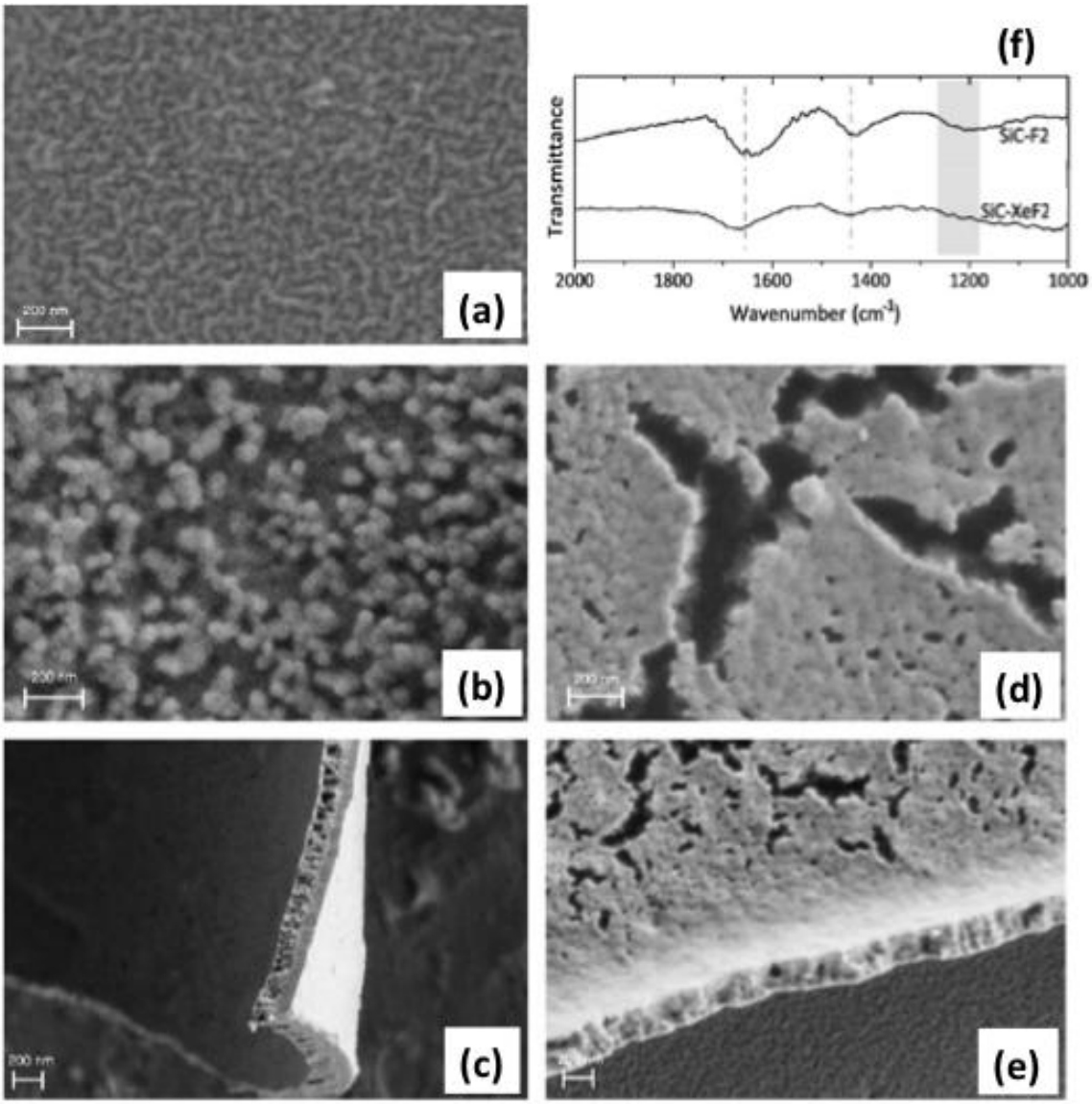

Fig. 7: SEM images of SiC carbide before fluorination (a), after fluorination under decomposition of XeF_2 (b,c) and after fluorination under F_2, (d,e); FTIR spectra of SiC carbide before fluorination, after fluorination with F_2 and XeF_2 (f).

4.4 Electrochemical materials such as $Li_4Ti_5O_{12}$

5. Conclusion

[1] W. Zhang, P. Bonnet, M ; Dubois, C. P. Ewels, K. Guérin, E. Petit,
J.-Y. Mevellec, L. Vidal, D. A. Ivanov, A. Hamwi, Comparative Study of SWCNT Fluorination by Atomic and Molecular Fluorine Chem. Mater. 2012, 24, 1744−1751

[2] Osuna, S.; Torrent-Sucarrat, M.; Sola, M.; Geerlings, P.; Ewels, C. P.; Van Lier, G. J. Phys. Chem. C 2010, 114, 3340.

[3] (a) Van Lier, G.; Ewels, C. P.; Zuliani, F.; De Vita, A.; Charlier, J.-C. J. Phys. Chem. B 2005, 109, 6153 ; (b) Kelly, K. F.; Chiang, I. W.; Mickelson, E. T.; Hauge, R. H.; Margrave, J. L.; Wang, X.; Scuseria, G. E.; Radloff, C.; Halas, N. J. Chem. Phys. Lett. 1999, 313, 445.
[4] Boltalina, O. V. J. Fluorine Chem. 2000, 101, 273.
[5] (a) Panich, A. M. Synth. Met. 1999, 100, 169 ; (b) Mallouk, T.; Hawkins, B. L.; Conrad, M. P.; Zilm, K.; Maciel, G. E.; Bartlett, N. Philos. Trans. R. Soc. London. Ser. A. 1985, 314, 179 ; (c) Dubois, M.; Giraudet, J.; Guérin, K.; Hamwi, A.; Fawal, Z.;
Pirotte, P.; Masin, F. J. Phys. Chem. B 2006, 110, 11800 ; (d) Giraudet, J.; Dubois, M.; Guérin, K.; Delabarre, C.; Hamwi, A.; Masin, F. J. Phys. Chem. B 2007, 111, 14143 ; (e) Giraudet, J.; Dubois, M.; Guérin, K.; Delabarre, C.; Hamwi, A.; Masin, F. J. Phys. Chem. B 2005, 109, 175 ; (f) Dubois, M.; Guérin, K.; Pinheiro, J. P.; Masin, F.; Fawal, Z.; Hamwi, A. Carbon 2004, 42, 1931 ; (g) Guérin, K.; Pinheiro, J. P.; Dubois, M.; Fawal, Z.; Masin, F.; Yazami, R.; Hamwi, A. Chem. Mater. 2004, 16, 1786.
[6] Sato, Y.; Itoh, K.; Hagiwara, R.; Fukunaga, T.; Ito, Y. Carbon. 2004, 42, 3243.
[7] W Zhang, Katia Guérin, M. Dubois, Z. El Fawal, D. A. Ivanov, L. Vidal, A. Hamwi Carbon nanofibres fluorinated using TbF4 as fluorinating agent. Part I: Structural properties, Carbon 46 (2008) 1010 –1016
[8] Chamssedine F, Dubois M, Guérin K, Giraudet J, Masin F, Ivanov DA, et al. Reactivity of carbon nanofibres with fluorine gas. Chem Mater 2007;19:161–72.
[9] Nakajima T, Watanabe N. Graphite fluorides and carbon–fluorine compounds. Boston: CRC Press; 1991.
[10] Lynum S, Hugdahl J, Hox K, Hildrum R, Nordvik M. patent EP1017622.
[11] Zhang W, Dubois M, Gue´rin K, Bonnet P, Petit E, Delpuech N, et al. Effect of graphitization on fluorination of carbon nanocones and nanodiscs. Carbon 2009;47(12):2763–75.
[12] (a) A. Magasinski, P. Dixon, B. Hertzberg, A. Kvit, J. Ayala, G. Yushin, Nat. Mater. 9 (2010) 353–358 ; (b) J.B. Donnet, R.P. Bansal, M.J. Wang, Carbon Black Science and Technology, second
ed., Marcel Dekker Inc., New York, NY, 1993.
[13] W. Zhang, M. Dubois, K. Guerin, P. Bonnet, H. Kharbache, F. Masin, A.P. Kharitonov, A. Hamwi, Phys. Chem. Chem. Phys. 12 (2010) 1388–1398.
[14] P. Thomas, J.L. Mansot, A. Molza, F. Begarin, M. Dubois, K. Guerin, Tribo. Lett. 56 (2009) 49-59.
[15] P. Thomas, D. Himmel, J.L. Mansot, M. Dubois, K. Guerin, W. Zhang, A. Hamwi, Tribo. Lett. 34 (2014) 259-271.
[16] J. Peyroux, M. Dubois, E. Tomasella, L. Frézet, A. P. Kharitonov, D. Flahaut, European Polymer Journal 66 (2015) 18–32
[17] (a) Nazarov V, Kondratov A, Stolyarov V, Evlampieva L, Baranov V, Gagarin M. Morphology of the surface layer of polymers modified by gaseous fluorine. Polym Sci Ser A 2006;48(11):1164–70 ; (b) Nansé G, Papirer E, Fioux P, Moguet F, Tressaud A. Fluorination of carbon blacks: an X-ray photoelectron spectroscopy study: I. A literature review of XPS studies of fluorinated carbons. XPS investigation of some reference compounds. Carbon 1997;35(2): 175–94 ; (c) Nansé G, Papirer E, Fioux P, Moguet F, Tressaud A. Fluorination of carbon blacks. An X-ray photoelectron spectroscopy study. Part II. XPS study of a furnace carbon black treated with gaseous fluorine at temperatures below 100 °C. Influence of the reaction parameters and of the activation of the carbon black on the fluorine fixation. Carbon 1997;35(3):371–88 ; (c) [49] Nansé G, Papirer E, Fioux P, Moguet F, Tressaud A. Fluorination of carbon blacks: an X-ray photoelectron spectroscopy study: III. Fluorination of different carbon blacks with gaseous fluorine at temperatures below 100 °C influence of the

morphology, structure and physico-chemical characteristics of the carbon black on the fluorine fixation. Carbon 1997;35(4):515–28.
[18] Carstens PAB, Marais SA, Thompson CJ. Improved and novel surface fluorinated products. J Fluorine Chem 2000;104(1):97–107.
[19] Kharitonov AP, Kharitonova LN. Surface modification of polymers by direct fluorination: a convenient approach to improve commercialproperties of polymeric articles. Pure Appl Chem 2009;81(3): 451–71.
[20] Kharitonov AP, Taege R, Ferrier G, Piven NP. The kinetics and mechanism of the direct fluorination of polyethylenes. Surf Coat Int Part B: Coat Trans 2005;88(3):201–12.
[21] (a) Sofo et al, Phys. Rev. B 75, 153401 2007. (b) Boukhvalov et al,J. Phys.: Condens. Matter 21, 344205 2009
[22] K. J. Jeon, Z. Lee, E. Pollak, L. Moreschini, A. Bostwick, C. M. Park, R. Mendelsberg, V. Radmilovic, R. Kostecki, T. J. Richardson and E. Rotenberg, Acs Nano, 2011, 5, 1042-1046.
[23] X. Wang, Y. Dai, J. Gao, J. Huang, B. Li, C. Fan, J. Yang and X. Liu, ACS Appl. Mater. Interfaces, 2013, 5, 8294-8299.
[24] (a) Z. Wang, J. Wang, Z. Li, P. Gong, X. Liu, L. Zhang, J. Ren, H. Wang and S. Yang, Carbon, 2012, 50, 5403-5410 ; (b) P. Gong, Z. Wang, Z. Li, Y. Mi, J. Sun, L. Niu, H. Wang, J. Wang and S. Yang, RSC Advances, 2013, 3, 6327-6330.
[25] M. S. Zhu, X. D. Xie, Y. L. Guo, P. L. Chen, X. W. Ou, G. Yu and M. H. Liu, Phys. Chem. Chem. Phys., 2013, 15, 20992-21000.
[26] P. W. Gong, Z. F. Wang, J. Q. Wang, H. G. Wang, Z. P. Li, Z. J. Fan, Y. Xu, X. X. Han and S. R. Yang, J. Mater. Chem., 2012, 22, 16950-16956
[27] (a) H. Chang, J. Cheng, X. Liu, J. Gao, M. Li, J. Li, X. Tao, F. Ding and Z. Zheng, Chemistry – A European Journal, 2011, 17, 8896-8903 ; (b) W. H. Lee, J. W. Suk, H. Chou, J. Lee, Y. Hao, Y. Wu, R. Piner, D. Akinwande, K. S. Kim and R. S. Ruoff, Nano Letters, 2012, 12, 2374-2378.
[28] (a) H. Chang, J. Cheng, X. Liu, J. Gao, M. Li, J. Li, X. Tao, F. Ding and Z. Zheng, Chemistry – A European Journal, 2011, 17, 8896-8903 ; (b) W. H. Lee, J. W. Suk, H. Chou, J. Lee, Y. Hao, Y. Wu, R. Piner, D. Akinwande, K. S. Kim and R. S. Ruoff, Nano Letters, 2012, 12, 2374-2378.
[29] A. C. Ferrari, Solid State Commun., 2007, 143, 47-57.
[30] (a) F. Withers, S. Russo, M. Dubois, M. F Craciun, Nanoscale Research letters, 6:526 (2011) ; (b) F. Withers, M. Dubois, A. K. Savchenko, Physical Review B 82 (2010) 073403
[31] J.H. Kaufman, S. Metin, D.D. Saperstein, Phys. Rev. B 39 (1989) 13053.
[32] A. Hamwi, M. Daoud, J.C. Cousseins, Synth. Met. 26 (1988) 89.
[33] Y.G. Gogotsi, I.-D. Jeon, M.J. McNallan, J. Mater. Chem. 7 (1997) 1841.